Alternating Conjugated Electron Donor–Acceptor Polymers Entailing Pechmann Dye Framework as the Electron Acceptor Moieties for High Performance Organic Semiconductors with Tunable...

ARTICLE *in* MACROMOLECULES · APRIL 2014

Impact Factor: 5.8 · DOI: 10.1021/ma5003694

7 AUTHORS, INCLUDING:

Zhengxu Cai
University of Chicago
19 PUBLICATIONS **240** CITATIONS
SEE PROFILE

Jianguo Wang
Gannan Normal University
19 PUBLICATIONS **230** CITATIONS
SEE PROFILE

Guanxin Zhang
Chinese Academy of Sciences
130 PUBLICATIONS **4,281** CITATIONS
SEE PROFILE

Zitong Liu
Chinese Academy of Sciences
35 PUBLICATIONS **277** CITATIONS
SEE PROFILE

Macromolecules

Article

pubs.acs.org/Macromolecules

Alternating Conjugated Electron Donor–Acceptor Polymers Entailing Pechmann Dye Framework as the Electron Acceptor Moieties for High Performance Organic Semiconductors with Tunable Characteristics

Zhengxu Cai, Hewei Luo, Penglin Qi, Jianguo Wang, Guanxin Zhang, Zitong Liu,* and Deqing Zhang*

Beijing National Laboratory for Molecular Sciences, CAS Key Laboratory of Organic Solids Institute of Chemistry, Chinese Academy of Sciences Beijing 100190, P. R. China

Supporting Information

ABSTRACT: In this paper, we report the design, synthesis and semiconducting behavior of two conjugated D–A polymers **P-BPDTT** and **P-BPDBT** which entail **BPD**, a Pechmann dye framework, as electron accepting moieties, and thieno[3,2-*b*]thiophene and 2,2′-bithiophene as electron donating moieties. Their HOMO/LUMO energies and bandgaps were estimated based on the respective cyclic voltammgrams and absorption spectra of thin films. **P-BPDTT** possesses lower LUMO level and narrower bandgap than **P-BPDBT**. On the basis of the characterization of the field-effect transistors, a thin film of **P-BPDTT** exhibits ambipolar semiconducting properties with hole and electron mobilities reaching 1.24 $cm^2 V^{-1} s^{-1}$ and 0.82 $cm^2 V^{-1} s^{-1}$, respectively, after thermal annealing. In comparison, thin film of **P-BPDBT** only shows *p*-type semiconducting behavior with hole mobility up to 1.37 $cm^2 V^{-1} s^{-1}$. AFM and XRD studies were presented to understand the interchain arrangements on the substrates and the variation of carrier mobilities.

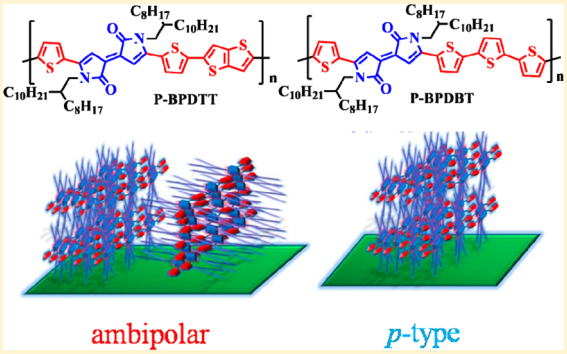

INTRODUCTION

Organic semiconducting materials have received increasing attentions in recent years because of their promising applications in various areas such as organic field-effect transistors (OFETs), organic light-emitting diodes (OLEDs), organic solar cells (OSCs), and sensors.[1] They also promise for applications in low-cost, large-area, and flexible electronic devices, such as radio frequency identification (RFID) tags, smart cards, and electronic papers.[2] So far, a number of organic semiconductors and resulting FETs with high carrier mobilities and good stabilities have been reported.[3] However, new organic semiconductors of even better performances are highly desirable in order to realize their practical applications in flexible electronic devices.[4] Compared to small molecules, conjugated polymers offer great advantages such as solution processability, good mechanical property and thermal stability.[5] Benefiting from new molecular design and device fabrication improvement, thin film transistors with conjugated polymers have made significant progresses in the past decade with carrier mobilities approaching or surpassing 2.0 $cm^2 V^{-1} s^{-1}$.[6]

Among the conjugated polymers those with alternating electron donor (D) and acceptor (A) units have been intensively investigated.[7] The studies reveal that intermolecular D–A interactions play an important role in these D–A conjugated polymers.[8] Therefore, semiconducting properties of these conjugated polymers are influenced significantly by the characteristics of electron donors and acceptors in these polymers.[9] Various electron acceptors have been successfully incorporated into D–A conjugated polymers to yield semiconductors with high carrier mobilities.[3] For instance, recently lots of conjugated D–A polymers, containing bis-amide-based electron acceptors, such as diketopyrrolopyrrole (**DPP**) and isoindigo (Scheme 1), were found to show high semi-

Scheme 1. Chemical Structures of Dithienyl-DPP, Dithienyl-BPD, and the Conjugated Polymers

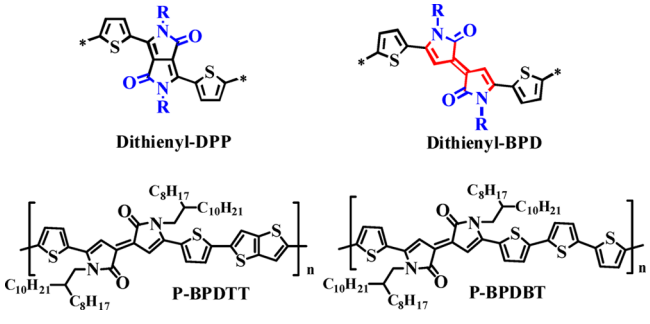

Received: February 18, 2014
Revised: April 6, 2014
Published: April 14, 2014

conducting performances with *p*-type, *n*-type and even ambipolar behaviors.[3,5,6] For instance, Yang, Oh, and their co-workers have recently disclosed a dithienyldiketopyrrolopyrrole−selenophene copolymer exhibiting ambipolar property with unprecedentedly high hole and electron mobilities of 8.84 $cm^2\ V^{-1}\ s^{-1}$ and 4.34 $cm^2\ V^{-1}\ s^{-1}$, respectively.[10] They also investigated thienoisoindigo-containing D−A polymers and the resulting polymers were found to show *p*-type and even ambipolar semiconducting behaviors with reasonably high carrier mobilities.[11] In comparison with electron donors, the choices of electron acceptors for constructing the D−A polymers are still limited.[3a−c]

In this paper we report two conjugated D−A polymers **P-BPDTT** and **P-BPDBT** (Scheme 1) which entail bipyrrolylidene-2,2′(1*H*,1′*H*)-dione (**BPD**) as electron acceptor moieties and thieno[3,2-*b*]thiophene or 2,2′-bithiophene as electron donating moieties. **BPD** is a derivative of Pechmann dye, which was first synthesized by Hans von Pechmann in 1882.[12] Being similar to **DPP** and isoindigo, it owns planar and polar structure with bis-amide as electron withdrawing units.[13] Alkyl chains can be introduced to amide groups to promote solubility.[14] Furthermore, **BPD** possesses narrow band gap and absorbs strongly in the region 450−720 nm. Some of us reported two small D−A−D molecules in which **BPD** units were flanked by two benzo[*b*]thiophene or benzo[*b*]furan moieties, and both of them were found to show *p*-type semiconducting properties with hole mobilities up to 1.4 $cm^2\ V^{-1}\ s^{-1}$ and high on/off ratio up to 10^6.[13] However, **BPD**-based conjugated D−A polymers were not described. It is anticipated that conjugated D−A polymers with **BPD** as the electron accepting moieties will have narrow bandgaps and tunable HOMO/LUMO energies, thus these BPD-containing D−A polymers may have tunable semiconducting characteristics. The results reveal that **P-BPDTT** with a narrow bandgap of 1.1 eV and LUMO of −3.7 eV exhibits ambipolar semiconducting properties with hole and electron mobilities reaching 1.24 $cm^2\ V^{-1}\ s^{-1}$ and 0.82 $cm^2\ V^{-1}\ s^{-1}$, respectively. In comparison, **P-BPDBT** only shows *p*-type semiconducting behavior with hole mobility up to 1.37 $cm^2\ V^{-1}\ s^{-1}$.

RESULTS AND DISCUSSION

Synthesis and Characterization. As depicted in Scheme 2, **P-BPDTT** and **P-BPDBT** were prepared by Stille cross-coupling of the respective bis(tin) reagents and compound **3** using $Pd_2(dba)_3$ as the catalyst. The synthesis started from compound **1** which was prepared according to the reported procedures.[15] Reaction of **1** with 2-octyldodecan-1-amine yielded **2** in 12.5% yield. Treatment of **2** with lithium diisopropylamide (LDA) at −78 °C, followed by addition of 1, 2-dibromo-tetrachloroethane led to **3** in 51% yield. **P-BPDTT** and **P-BPDBT** were precipitated out from the reaction mixture after addition of methanol. The precipitates were subjected to Soxhlet extraction with methanol, hexane, acetone, and chloroform to remove the respective monomers and oligomers.[16] The resulting residues were collected and dried under vacuum to afford **P-BPDTT** and **P-BPDBT** in 95% and 74.5% yields, respectively. The chemical structures of **P-BPDTT** and **P-BPDBT** were verified by ^1H NMR, solid-state ^{13}C NMR and elemental analysis (see Experimental Section).

P-BPDTT and **P-BPDBT** are only soluble in *o*-dichlorobenzene and 1,1,2,2-tetrachloroethane. The weight-average molecular weights of the **P-BPDTT** and **P-BPDBT** were determined by gel permeation chromatography (GPC) at 150 °C using polystyrenes as standard with 1,2,4-trichlorobenzene as eluent. M_w of **P-BPDTT** and **P-BPDBT** are 16 kg·mol^{-1} and 10 kg·mol^{-1} with polydispersities of 2.08 and 2.22, respectively. On the basis of the TGA curves shown in Figure S1, the decomposition temperatures of **P-BPDTT** and **P-BPDBT** are higher than 250 °C at 5% weight loss.

Scheme 2. Synthetic Routes to P-BPDTT and P-BPDBT[a]

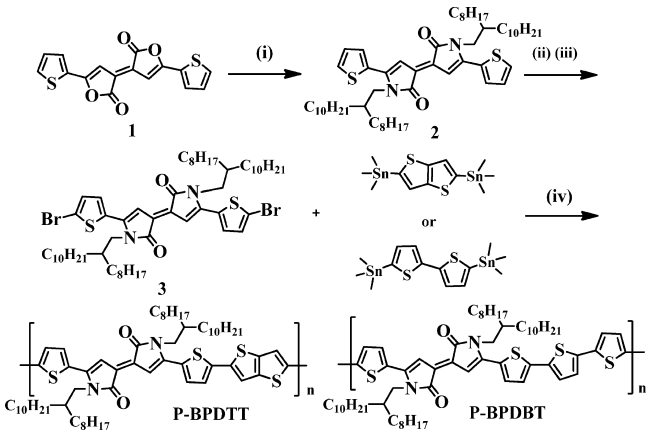

[a]Reagents and conditions: (i) 2-octyldodecan-1-amine, CH_2Cl_2, room temperature, 12 h; HCl (2.0 M); (ii) lithium diisopropylamide, −78 °C, 30 min; (iii) 1,2-dibromotetrachloroethane, −78 °C, 60 min; (iv) thieno[3,2-*b*]thiophene-2,6-diylbis(trimethylstannane) or 5,5′-bis-(trimethylstannyl)-2,2′-bithiophene, $Pd_2(dba)_3$, $P(o\text{-tol})_3$, toluene, 100 °C, 24 h.

HOMO/LUMO Energies and Bandgaps. Cyclic voltammgrams of **P-BPDTT** and **P-BPDBT** were measured in the form of thin films. As depicted in Figure S2, both polymers possess irreversible oxidation and reduction waves. On the basis of the respective onset oxidation and reduction potentials (see Table 1), HOMO and LUMO energies of **P-BPDTT** and **P-BPDBT** were estimated with the following equations: HOMO = $-(E_{ox}^{onset} + 4.4)$ eV; LUMO = $-(E_{red}^{onset} + 4.4)$ eV. As listed in Table 1, the HOMO/LUMO levels of **P-BPDTT** are −5.0 and −3.7 eV, respectively, whereas the HOMO/LUMO levels of **P-BPDBT** are −5.0 eV and −3.6 eV, respectively. HOMO energies of **P-BPDTT** and **P-BPDBT** were measured with ultraviolet photoelectron spectroscopy (UPS). On the basis of the data shown in Figure S3, HOMO energies of **P-BPDTT** and **P-BPDBT** were determined to be −4.8 and −4.9 eV, respectively, which are close to those on the basis of the onset oxidation potentials. These results manifest that HOMO/LUMO levels of such **BPD**-containing polymers can be slightly modulated by the respective electron donating moieties: thieno[3,2-*b*]thiophene in **P-BPDTT** and 2,2′-bithiophene in **P-BPDBT**. **P-BPDTT** possesses slightly lower LUMO levels (thus narrower bandgap) compared to **P-BPDBT**.

Figure 1 shows the absorption spectra of the solutions and thin films of **P-BPDTT** and **P-BPDBT**. Both solutions and thin-films of **P-BPDTT** and **P-BPDBT** exhibit wide absorptions extending to 1200 nm. **P-BPDTT** and **P-BPDBT** in solutions absorb strongly around 834 and 790 nm, and the absorptions of their thin-films are obviously red-shifted in comparison with those in solutions as shown in Figure 1. For instance, the absorption bands at 834 nm in solutions are red-shifted to 858 nm for the thin-films of **P-BPDTT**. Such absorption spectral shifts may be ascribed to the intermolecular interactions within thin films of **P-BPDTT** and **P-BPDBT** which may entail the intermolecular electron-donor and

dx.doi.org/10.1021/ma5003694 | *Macromolecules* 2014, 47, 2899−2906

Table 1. Absorption Maxima, Redox Potentials, HOMO/LUMO Energies, and Bandgaps of P-BPDTT and P-BPDBT

	λ_{max} (nm)				expt[b] (calcd)[c]			
polymer	solution[a]	film	E_{ox}^{onset} (V)	E_{red}^{onset} (V)	HOMO (eV)	LUMO (eV)	band gap (eV)[d]	E_{IP}^{UPS} (eV)[e]
P-BPDTT	444, 834	450, 858	0.6	−0.7	−5.0 (−4.6)	−3.7 (−3.0)	1.1	−4.8
P-BPDBT	454, 790	468, 815	0.6	−0.8	−5.0 (−4.6)	−3.6 (−3.0)	1.2	−4.9

[a]Measured in $CHCl_2CHCl_2$ solutions of **P-BPDTT** (1.0×10^{-5} M) and **P-BPDBT** (1.0×10^{-5} M). [b]based on the respective onset oxidation and reduction potentials of **P-BPDTT** and **P-BPDBT** with the following equations: LUMO = $-(E_{red}^{onset} + 4.4)$ eV; HOMO = $-(E_{ox}^{onset} + 4.4)$ eV. [c]Based on the DFT calculations. [d]Based on the absorption spectral data. [e]Based on redox potentials. determined by UPS. $E_{IP}^{UPS} = h\nu - (E_{cutoff1} - E_{cutoff2})$, incident photon energy ($h\nu$ = 21.2 eV) for He I.

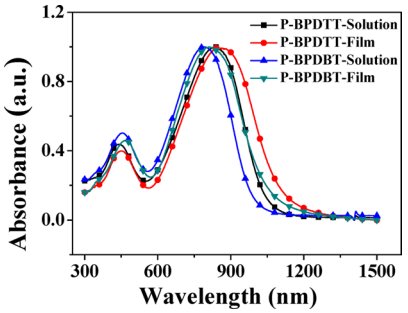

Figure 1. Normalized absorption spectra for solutions of **P-BPDTT** (1.0×10^{-5} M in $CHCl_2CHCl_2$) and **P-BPDBT** (1.0×10^{-5} M in $CHCl_2CHCl_2$) and their thin films.

-acceptor interactions. On the basis of the respective onset absorptions, the corresponding optical bandgaps were estimated to be 1.1 and 1.2 eV for **P-BPDTT** and **P-BPDBT**, respectively. These optical bandgaps are slightly different from those on the basis of the cyclic voltammetric data. But, **P-BPDTT** owns narrower bandgap than **P-BPDBT**, which is consistent with the electrochemical data (see above).

To provide more insights into the structural and electronic features of the alternating D−A polymers **P-BPDTT** and **P-BPDBT**, DFT calculations at the B3LYP/6-31G(d,p) level were performed for each two repeated units in **P-BPDTT** and **P-BPDBT**. As depicted in Figure 2, both the HOMO and LUMO orbitals of these two conjugated polymers are well distributed over their conjugated backbones. Moreover, the backbones of **P-BPDTT** and **P-BPDBT** are almost coplanar. Such structural features are beneficial for enhancing intermolecular interactions and widening absorptions. The uniform distribution of their HOMO/LUMO orbitals among the conjugated backbones implies that interactions exist among **BPD** and the electron donating moieties. Their HOMO/LUMO energies were also calculated, which are different from the experimental data (see Table 1) because the solvent effects were not included in the calculations.

Thin Film Field-Effect Transistors. Bottom-gate/bottom-contact field-effect transistors (FETs) with thin-films of **P-BPDTT** and **P-BPDBT** were fabricated with conventional techniques (see Experimental Section). The device performances were measured under nitrogen atmosphere. Figure 3 shows the transfer and output characteristics of FETs with thin films of **P-BPDTT** and **P-BPDBT** after thermal annealing.[17] Thus, thin film of **P-BPDTT** exhibits ambipolar semiconducting behavior under nitrogen atmosphere,[18] whereas thin film of **P-BPDBT** behaves as a *p*-type semiconductor. The hole (μ_h) and electron (μ_e) mobilities of the as-prepared FETs based on **P-BPDTT** were measured to be 0.4 $cm^2\ V^{-1}\ s^{-1}$ and 0.013 $cm^2\ V^{-1}\ s^{-1}$, respectively; moreover, both μ_h and μ_e were enhanced by removing the *o*-dichlorobenzene solvent at 120 °C in vacuum for 2.0 h. To our delight, further thermal annealing led to boosting both hole and electron mobilities (see Table 2); μ_h and μ_e reached 1.24 $cm^2\ V^{-1}\ s^{-1}$ and 0.82 $cm^2\ V^{-1}\ s^{-1}$, respectively, after annealing at 200 °C.[19] But, μ_h and μ_e started to decrease after further thermal annealing at 240 °C.

Furthermore, by considering the ambipolar nature of **P-BPDTT** which also show balanced and relatively high hole and electron mobilities, two identical transistors with thin films of **P-BPDTT** were combined into an inverter circuit (see Figure S6). Figure S6 also shows the output (V_{OUT}) as a function of the input voltage (V_{IN}) at constant supply bias (V_{DD}). Inverting functionality is clearly observed. From the steepness of inverter

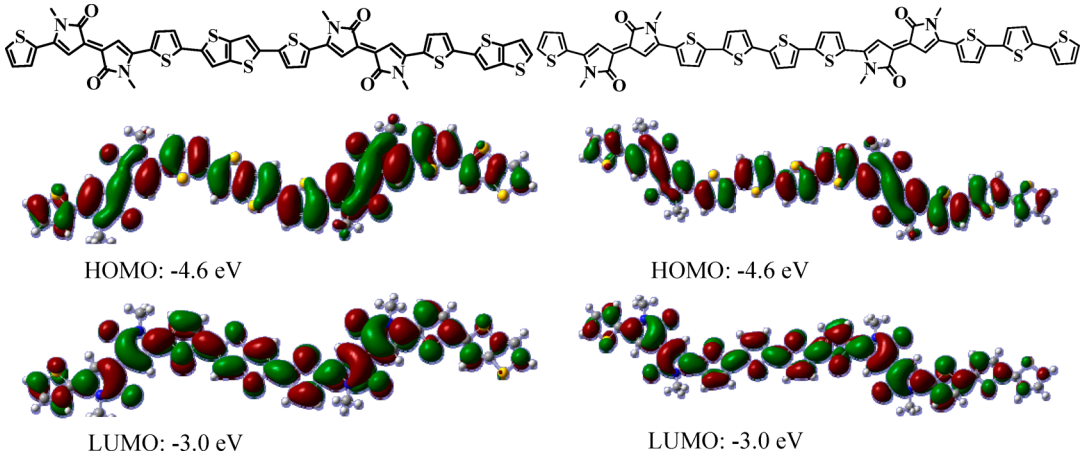

Figure 2. Calculated molecular orbitals and HOMO/LUMO energies of two repeated units of **P-BPDTT** (left) and **P-BPDBT** (right) at the B3LYP/6-31G(d,p) level. The alkyl chains are replaced with methyl groups for computational simplicity.

dx.doi.org/10.1021/ma5003694 | *Macromolecules* 2014, 47, 2899−2906

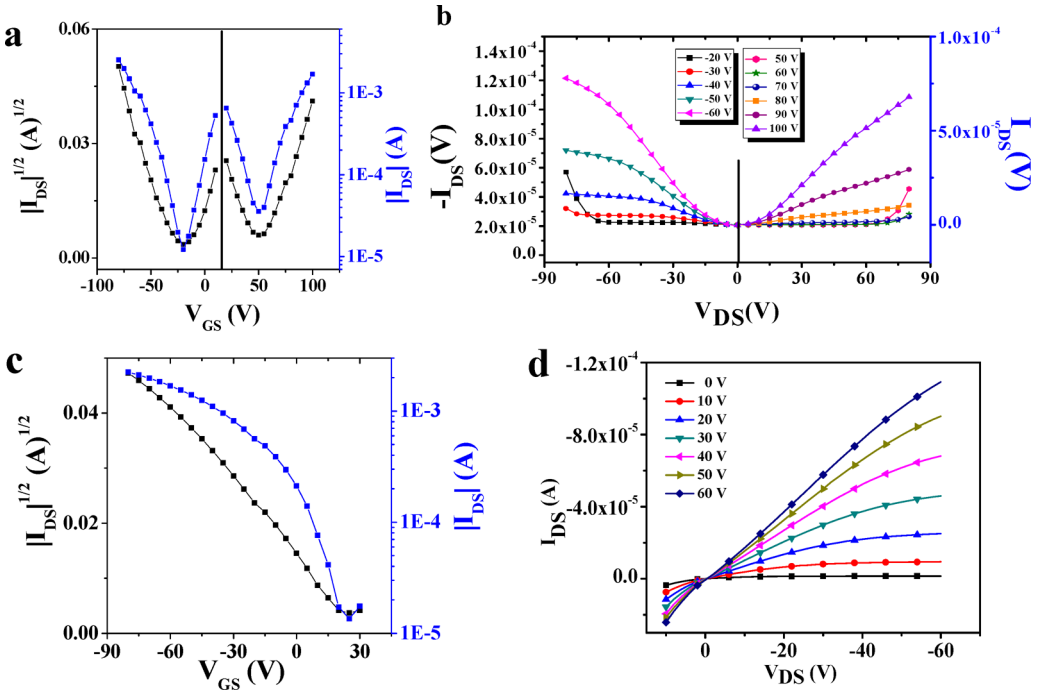

Figure 3. Transfer and output characteristics of OFET devices based on **P-BPDTT** (a and b) annealed at 200 °C (V_{DS} for transfer characteristics are −100 and +100 V, respectively); the channel width (W) and length (L) were 1400 and 5 μm, respectively; the transfer and output characteristics for OFET with **P-BPDBT** (c and d) after annealing at 120 °C; the channel width (W) and length (L) were 1400 and 10 μm, respectively.

Table 2. Hole and Electron Mobilities, Threshold Voltages (V_{th}), and On/Off Ratios ($I_{on/off}$) for FETs Based on Thin-Films of P-BPDTT and P-BPDBT with OTS-Modified Si/SiO_2 Substrates and Unmodified Au as Electrodes at Different Annealing Temperatures[a]

compd	temp (°C)	μ_h (cm^2 V^{-1} s^{-1})	$I_{on/off}$	V_{th} (V)	μ_e (cm^2 V^{-1} s^{-1}	$I_{on/off}$	V_{th} (V)
P-BPDTT	25	0.1−0.4	10^2−10^3	11−14	0.008−0.013	10	48−51
	120	0.4−0.85	10^2−10^3	8−15	0.09−0.35	10	48−54
	160	0.45−0.75	10^3	8−15	0.14−0.30	10	49−55
	200	0.73−1.24	10^3	6−15	0.43−0.82	10^2	49−58
	240	0.68−1.22	10^2	8−14	0.16−0.30	10	52−64
P-BPDBT	25	0.013−0.067	10^4	10−12	–	–	–
	120	0.45−1.37	10^2−10^3	23−33	–	–	–
	160	0.33−0.42	10^3	9−15	–	–	–
	200	0.3−0.47	10^3	9−21	–	–	–

[a]The data were obtained based on more than 10 devices.

curve, the gain was estimated to be estimated to be 33, which is relatively high for inverters based on organic semiconductors.[20]

P-BPDBT behaves as a *p*-type semiconductor. Hole mobilities of FETs with thin-films of **P-BPDBT** can be enhanced after thermal annealing at different temperatures (Table 2). The as-prepared FET of **P-BPDBT** exhibits hole mobility of 0.067 cm^2 V^{-1} s^{-1} and on/off ratio ($I_{on/off}$) of 10^4. μ_h increases to 1.37 cm^2 V^{-1} s^{-1} after annealing at 120 °C. But, μ_h decreases to 0.42 cm^2 V^{-1} s^{-1} after annealing at 160 °C. The variation of μ_h after thermal annealing is in agreement with the respective morphological changes observed for thin films of **P-BPDBT** (see below).

Thin films of **P-BPDTT** and **P-BPDBT** before and after thermal annealing were characterized by AFM and XRD in order to understand the variation of the carrier mobilities. Figure 4 shows the AFM images of the as-prepared thin-films of **P-BPDTT** and **P-BPDBT** and those after thermal annealing. The as-prepared thin-film of **P-BPDTT** contains molecular domains which are transformed into larger ones and became more interconnected after thermal annealing at 200 °C. The root-mean-square roughness (R_{RMS}) is changed from 0.44 to 0.56, which may indicate the increase of the crystallization and ordering of polymeric chains after thermal annealing. In comparison, the thin film morphology of **P-BPDBT** is not significantly altered after thermal annealing.

Figure 5 shows the out-of-plane and in-plane X-ray diffraction patterns of thin films of **P-BPDTT** and **P-BPDBT** before and after thermal annealing. Three weak diffraction signals at 2θ = 4.24° (out-of-plane), 2θ = 24.47° (broad, out-of-plane) and 2θ = 4.04° (in plane), corresponding *d*-spacing of 20.82 Å, 3.63 and 21.84 Å, were detected for the as-prepared thin film of **P-BPDTT**. After thermal annealing at 200 °C, the intensity of the signal at 2θ = 4.24° was enhanced, and a new broad diffraction signal at 2θ = 20.57° (out-of-plane), corresponding to a *d*-spacing of 4.31 Å, emerged. On the basis of these diffraction data, it may be concluded that (1) both edge-on and face-on intermolecular arrangements exist for **P-BPDTT** on the OTS modified substrate as illustrated in

dx.doi.org/10.1021/ma5003694 | *Macromolecules* 2014, 47, 2899−2906

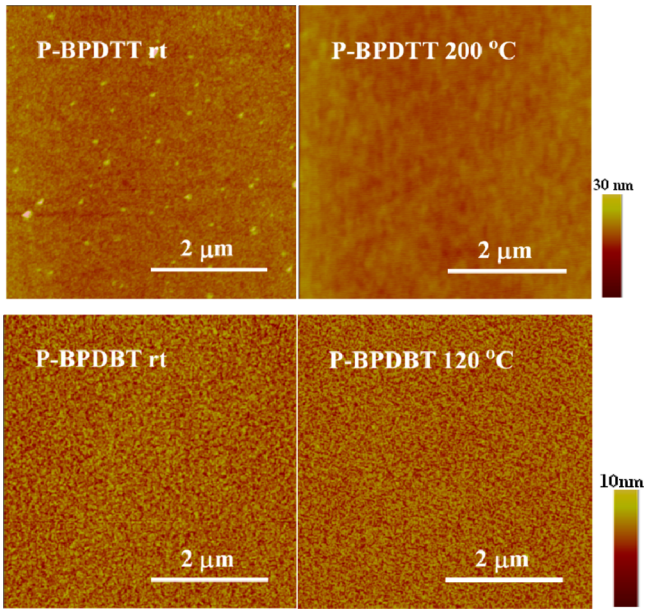

Figure 4. AFM images for thin-films of **P-BPDTT** and **P-BPDBT** (as-prepared and after thermal annealing).

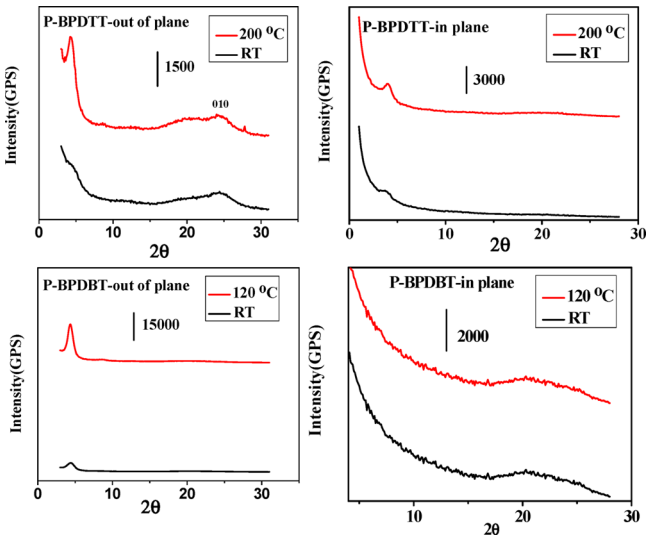

Figure 5. Grazing incidence X-ray diffraction patterns of **P-BPDTT** and **P-BPDBT**.

Scheme 3. By considering the fact that the *d*-spacing corresponding to $2\theta = 4.24°$ and $2\theta = 4.04°$, is shorter than the length of the BPD moiety along the fully extended alkyl chain direction (ca. 30 Å), the side alkyl chains are closely interdigitated in adjacent layers. The appearance of $2\theta = 24.47°$ (3.63 Å) and $2\theta = 20.57°$ (4.31 Å) implies the interchain $\pi-\pi$ interactions among the electron donating and accepting moieties. (2) The slight intensity enhancement for the signal at $2\theta = 4.24°$ and the appearance of the diffraction peak at $2\theta = 20.57°$ indicate the increase of the crystallinity for the thin film of **P-BPDTT** after thermal annealing at 200 °C. This is indeed in agreement with the observation that both hole and electron mobilities are enhanced after thermal annealing (see Table 2).

Scheme 3. Schematic Illustration of the Inter-Chain Arrangements for P-BPDTT (left) and P-BPDBT (right) on the Substrates

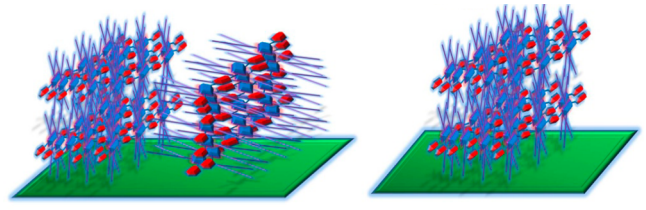

The as-prepared thin film of **P-BPDBT** shows a weak diffraction peak at 4.32°, corresponding to a *d*-spacing of 20.43 Å in the out-of-plane diffraction pattern. A rather weak and broad diffraction signal around 21°, corresponding to *d*-spacing of 4.22 Å, was detected in the in-plane diffraction pattern for the as-prepared thin film of **P-BPDBT**. After thermal annealing at 120 °C, the intensity for the diffraction signals increase slightly. These XRD data indicate that polymer chains are predominantly arranged in edge-on manner on the substrate as illustrated in Scheme 3. The alkyl chains are also interdigitated and interchain $\pi-\pi$ interactions exist within thin film of **P-BPDBT**.

The incorporation of two different electron-donating moieties (thieno[3,2-*b*]thiophene and 2,2′-bithiophene) into these two conjugated polymers is expected to tune their electronic structures, HOMO/LUMO levels, solid-state morphologies and the nature of charge-transport.[21] As listed in Table 1, HOMO levels of both **P-BPDTT** and **P-BPDBT** are relatively high, but the LUMO level of **P-BPDTT** is slightly lower than that of **P-BPDBT**. Additionally, these two different electron donating moieties may affect the respective interchain interactions, thin-film morphologies as well as interfacial properties. These facts may explain that **P-BPDBT** exhibits dominant hole-transport properties, while **P-BPDTT** shows balanced hole- and electron-transport properties.

The relatively high carrier mobilities of thin films of **P-BPDTT** and **P-BPDBT** may be attributed to the following facts: (1) **BPD** is a planar electron acceptor moiety. In fact, small **BPD**-containing conjugated D−A molecules were found to show high carrier mobilities;[13] (2) thin films of both **P-BPDTT** and **P-BPDBT** exhibit good crystallinity in terms of $\pi-\pi$ stacking of conjugated backbones and lamella packing of alkyl side chains based on XRD studies. This is indeed in agreement with the theoretical investigations[22] which indicate that the carrier mobilities of conjugated polymers are controlled by the electronic structures of polymer backbones and interchain packing as well as the crystalline order of alkyl side chains.

■ CONCLUSIONS

In this paper, we successfully incorporated **BPD**, a Pechmann dye framework, into conjugated alternating D−A polymers as electron-accepting moieties. The two conjugated polymers **P-BPDTT** and **P-BPDBT** that entail thieno[3,2-*b*]thiophene and 2,2′-bithiophene as electron-donating moieties, respectively, can be solution-processed and possess low bandgaps of 1.1−1.2 eV based on the electrochemical and absorption spectral data. FETs with thin films of **P-BPDTT** and **P-BPDBT** were fabricated with conventional techniques. The results reveal that thin film of **P-BPDTT** exhibits ambipolar semiconducting properties with hole and electron mobilities reaching 1.24 $cm^2 V^{-1} s^{-1}$ and 0.82 $cm^2 V^{-1} s^{-1}$, respectively, after thermal annealing. In comparison, thin film of **P-BPDBT** only shows *p*-type semiconducting behavior with hole mobility up to 1.37

dx.doi.org/10.1021/ma5003694 | *Macromolecules* 2014, 47, 2899−2906

$cm^2\ V^{-1}\ s^{-1}$. XRD studies imply that thin films of **P-BPDTT** and **P-BPDBT** adopt different interchain arrangements on the substrates. Current studies demonstrate that **BPD**, a planar and polar electron accepting moiety, can be utilized as to construct conjugated D−A polymers for high performance semiconductors. Additionally, such conjugated polymers are potentially interesting for photovoltaic materials by considering the fact that these **BPD**-containing polymers possess low bandgaps. Further investigations include the design and synthesis of new **BPD** frameworks with low HOMO/LUMO levels which are required for air-stable semiconductors.

EXPERIMENTAL SECTION

Materials and Characterization Techniques. The reagents and starting materials were commercially available and used without any further purification if not specified elsewhere. Compound **1** was synthesized according to the previous report.[15] ^{1}H NMR and ^{13}C NMR spectra were recorded on Bruker AVANCE III 300 MHz spectrometer, Bruker AVANCE III 400 MHz spectrometer and Bruker AVANCE III 600 MHz spectrometer. MALDI-TOF MS spectra were recorded with BEFLEX III spectrometer. Elemental analysis was performed on a Carlo Erba model 1160 elemental analyzer. Solution and thin films absorption spectra were measured with JASCO V-570 UV−vis spectrophtometer. TGA (SHIMADZU DTG-60) measurements were performed under nitrogen atmosphere at a heating rate of 10 K/min. Cyclic voltammetric measurements were carried out in a conventional three-electrode cell using Pt wires of 2 mm diameter as working and counter electrodes, and an Ag/AgCl reference electrode on a computer-controlled CHI660C instruments at room temperature; n-Bu_4NPF_6 was used as the conducting electrolyte. Ultraviolet photoelectron spectroscopy was measured by AXIS ULTRA DLD with the illuminant of He I. The GIXRD data were obtained at 1W1A, Beijing Synchrotron Raidation Facility. The thin-films were imaged in air using a Digital Instruments Nanoscope V atomic force microscope (AFM) operated in tapping mode with a Nanoscope V instrument.

Synthesis of Compound 2. Compound **1** (2.19 g, 6.68 mmol) and 2-octyldodecan-1-amine (5.80 g, 19.5 mmol) were dissolved in CH_2Cl_2 (80 mL) at room temperature and the mixture was stirred for 12 h to form a clear solution. Then, 10 mL of HCl (2 mol/L) was added, and the reaction mixture turned blue immediately. After separation, the organic layer was washed with saturated $NaHCO_3$, dried over sodium sulfate. The residue was purified by column chromatography with the mixture of petroleum ether (60−90 °C) and CH_2Cl_2 (5:1, v/v) as the eluent. Compound **2** was obtained as dark blue solids (732 mg, 12.5%). ^{1}H NMR (400 MHz; $CDCl_3$; δ): 7.45 (d, 2H, J = 4.8 Hz), 7.41 (d, 2H, J = 3.6 Hz), 7.13 (dd, 2H, J = 3.6 Hz, J = 4.0 Hz), 7.09 (s, 2H), 3.78 (d, 4H, J = 7.6 Hz), 1.64 (m, 2H), 1.20 (m, 64H), 0.88−0.84 (m, 12H). ^{13}C NMR (100 MHz, $CDCl_3$, δ): 171.3, 145.6, 133.7, 128.6, 128.4, 128.3, 128.2, 103.9, 45.5, 37.8, 32.3, 32.2, 31.6, 30.3, 30.0, 29.9, 29.8, 29.7, 29.7, 26.6, 23.1, 23.0, 14.5. MALDI−TOF m/z: 887.7 [M^+]. Anal. Calcd for $C_{56}H_{90}N_2O_2S_2$: C, 75.79; H, 10.22; N, 3.16; S, 7.23. Found: C, 75.91; H, 10.17; N, 3.29; S, 7.10.

Synthesis of Compound 3. Lithium diisopropylamide (1.14 mL, 1.8 M solution in THF/n-heptanes/ethylbenzene) was added to a solution of compound **2** (726 mg, 0.82 mmol) in dry THF (50 mL) at −78 °C. The resulting solution was stirred for 30 min under nitrogen and then 1,2-dibromotetrachloroethane (798 mg, 2.45 mmol) in THF (5 mL) was added dropwise. After stirred for additional 1.0 h, 10 mL of water was added to the reaction mixture which was extracted with CH_2Cl_2 (3 × 50 mL). The organic layer was washed with saturated brine, dried over sodium sulfate and evaporated to dryness. The residue was purified by column chromatography with petroleum ether (60−90 °C) and CH_2Cl_2 (5:1, v/v) as the eluent. Compound **2** was obtained as dark blue solids (436 mg, 51%). ^{1}H NMR (400 MHz, $CDCl_3$, δ): 7.16 (d, 2H, J = 4 Hz), 7.08 (d, 2H, J = 4 Hz), 7.02 (s, 2H), 3.72 (d, 4H, J = 8 Hz), 1.63 (m, 2H), 1.21−1.18 (m, 64H), 0.88−0.86 (m, 12H). ^{13}C NMR (100 MHz, $CDCl_3$, δ): 171.0, 144.6, 135.1, 131.4, 128.5, 128.3, 116.1, 104.1, 45.5, 37.8, 32.8, 32.3, 31.5, 30.3, 29.9, 29.8, 29.7, 29.6, 26.6, 23.1, 14.5. MALDI−TOF m/z: 1045.4 [M + H^+], 1067.4 [M + Na^+]. Anal. Calcd for $C_{56}H_{88}Br_2N_2O_2S_2$: C, 64.35; H, 8.49; N, 2.68; S, 6.14. Found: C, 64.16; H, 8.39; N, 2.56; S, 6.16.

Synthesis of P-BPDTT. Compound **3** (130 mg, 0.12 mmol) and 2,5-bis(trimethylstannyl)thieno[3,2-b]thiophene (59 mg, 0.12 mmol) were taken into a Schlenk tube under nitrogen atmosphere with 10 mL of anhydrous toluene. Then tris(dibenzylideneacetone)dipalladium(0) ($Pd_2(dba)_3$) (2.3 mg) and tri(o-tolyl)phosphine ($P(o\text{-tol})_3$) (3.0 mg) were added in one portion. The tube was charged with nitrogen through a freeze−pump−thaw cycle for three times. The mixture was stirred for 24 h at 90 °C under nitrogen. After cooling to room temperature, the highly viscous black gel-like solution was poured into methanol and the resulting precipitate was filtered. The polymer was purified by Soxhlet extraction using methanol, acetone, hexane and chloroform sequentially. The residue was collected and dried under vacuum to afford polymer (120 mg, 95%). ^{1}H NMR (400 MHz, $CDCl_2CDCl_2$, δ): 7.41−7.28 (m, 2H), 7.19−7.18 (m, 2H), 7.12−6.96 (m, 4H), 3.82 (s, 4H), 1.22 (m, 66H), 0.85 (m, 12H). ^{13}C NMR (100 MHz, solid, δ): 171.0, 139.7, 135.5, 134.6, 130.5, 125.2, 115.4, 114.2, 104.3, 38.9, 32.8, 30.7, 23.7, 15.1. GPC: M_n = 7.2 kDa, M_w = 16 kDa, PDI = 2.22. Anal. Calcd for $C_{62}H_{90}N_2O_2S_4$: C, 72.75; H, 8.86; N, 2.74; S, 12.53. Found: C, 70.91; H, 8.58; N, 2.65; S, 11.92.

Synthesis of P-BPDBT. Compound **3** (150 mg, 0.14 mmol) and 5,5′-bis(trimethylstannyl)-2,2′-bithiophene (71 mg, 0.14 mmol) were taken in a Schlenk tube under nitrogen atmosphere with 10 mL of anhydrous toluene. Tris(dibenzylideneacetone)dipalladium (0) ($Pd_2(dba)_3$) (2.5 mg) and tri(o-tolyl)phosphine ($P(o\text{-tol})_3$) (3.5 mg) were added in one portion. The tube was charged with nitrogen through a freeze−pump−thaw cycle for three times. The mixture was stirred for 24 h at 90 °C under nitrogen. After cooling to room temperature, the highly viscous black gel-like solution was poured into methanol and the resulting precipitate was filtered. The polymer was purified by Soxhlet extraction using methanol, acetone, hexane and chloroform sequentially. The residue was collected and dried under vacuum to afford polymer (112 mg, 75%). ^{1}H NMR (400 MHz, $CDCl_2CDCl_2$, δ): 7.39 (m, 2H), 7.33−6.69 (m, 10H), 3.81 (m, 4H), 1.22 (m, 66H), 0.86 (m, 12H). ^{13}C NMR (100 MHz, solid, δ): 170.5, 136.6, 131.2, 129.6, 125.0, 104.2, 38.0, 32.8, 30.8, 23.7, 15.1. GPC: M_n = 4.8 kDa, M_w = 10 kDa, PDI = 2.08. Anal. Calcd for $C_{64}H_{92}N_2O_4S_2$: C, 73. 23; H, 8.83; N, 2.67, S, 12.22. Found: C, 71.32; H, 8.31; N, 2.59; S, 11.68.

Fabrication of OFET Devices. A heavily doped n-type Si wafer and a layer of dry oxidized SiO_2 (300 nm, with roughness lower than 0.1 nm and capacitance of 11 nF cm^{-2}) were used as a gate electrode and gate dielectric layer, respectively. The drain-source (D-S) gold contacts were fabricated by photolithography. The substrates were cleaned in water, deionized water, alcohol, and rinsed in acetone. Then, the surface was modified with n-trichloro(octadecyl)silane (OTS). After that, the substrates were cleaned in n-hexane, $CHCl_3$ and EtOH sequentially. **P-BPDTT** and **P-BPDBT** were dissolved in hot o-1,2-dichlorobenzene (3.0 mg/mL) and spin-coated on above substrate at 2000 rpm for 60 s. The annealing process was carried out in vacuum for 2.0 h at each temperature. Field-effect characteristics of the devices were determined by using a Keithley 4200 SCS semiconductor parameter analyzer.

ASSOCIATED CONTENT

Supporting Information

Characterization techniques, TGA, cyclic voltammetry, ultraviolet photoelectron spectroscopy, density functional theory calculations, characterization of OFETs, and ^{1}H NMR and ^{13}C NMR data. This material is available free of charge via the Internet at http://pubs.acs.org.

AUTHOR INFORMATION

Corresponding Authors

*(D.Z.) E-mail: dqzhang@iccas.ac.cn.

*(Z.L.) E-mail: drzitong@gmail.com.

Notes

The authors declare no competing financial interest

■ ACKNOWLEDGMENTS

The GIXRD data were measured at 1W1A, Beijing Synchrotron Radiation Facility. The authors gratefully acknowledge the assistance of scientists of Diffuse X-ray Scattering Station during the experiments. The present research was financially supported by Chinese Academy of Sciences, the NSFC, and the State Key Basic Research Program.

■ REFERENCES

(1) (a) Mitsui, C.; Soeda, J.; Miwa, K.; Tsuji, H.; Takeya, J.; Nakamura, E. *J. Am. Chem. Soc.* **2012**, *134*, 5448. (b) Schmidt, R.; Oh, J. K.; Sun, Y.-S.; Deppisch, M.; Krause, A.-M.; Radacki, K.; Braunschweig, H.; Könemann, M.; Erk, P.; Bao, Z. N.; Würthner, F. *J. Am. Chem. Soc.* **2009**, *131*, 6215. (c) Gao, Y.; Yip, H.-L.; Chen, K.-S.; O'Malley, K. M.; Acton, O.; Sun, Y.; Guy, T.; Chen, H. Z.; Jen, A. K.-Y. *Adv. Mater.* **2011**, *23*, 1903. (d) Cao, Y.; Steigerwald, M. L.; Nuckolls, C.; Guo, X. *Adv. Mater.* **2010**, *22*, 20. (e) Li, L. Q.; Gao, P.; Schuermann, K. C.; Ostendorp, S.; Wang, W. C.; Du, C.; Lei, Y.; Fuchs, H.; De Cola, L.; Müllen, K.; Chi, L. F. *J. Am. Chem. Soc.* **2010**, *132*, 8807. (f) Cai, Z. X.; Zhang, H. T.; Geng, H.; Liu, Z. T.; Yang, S. F.; Luo, H. W.; Jiang, L.; Peng, Q.; Zhang, G. X.; Chen, J.; Yi, Y. P.; Hu, W. P.; Zhang, D. Q. *Chem.—Eur. J.* **2013**, *19*, 14573. (g) Liang, Z. X.; Tang, Q.; Mao, R. X.; Liu, D. Q.; Xu, J. B.; Miao, Q. *Adv. Mater.* **2011**, *23*, 5514. (h) Sirringhaus, H. *Adv. Mater.* **2014**, *26*, 1319. (i) Rochat, S.; Swager, T. M. *J. Am. Chem. Soc.* **2013**, *135*, 17703.

(2) (a) Murphy, A. R.; Fréchet, J. M. J. *Chem. Rev.* **2007**, *107*, 1066. (b) Zaumseil, J.; Sirringhaus, H. *Chem. Rev.* **2007**, *107*, 1296. (c) Anthony, J. E.; Facchetti, A.; Heeney, M.; Marder, S. R.; Zhan, X. W. *Adv. Mater.* **2010**, *22*, 3876. (d) Wang, C. L.; Dong, H. L.; Hu, W. P.; Liu, Y. Q.; Zhu, D. B. *Chem. Rev.* **2012**, *112*, 2208. (e) He, T.; Stolte, M.; Würthner, F. *Adv. Mater.* **2013**, *25*, 6951. (f) Takimiya, K.; Shinamura, S.; Osaka, I.; Miyazaki, E. *Adv. Mater.* **2011**, *23*, 4347. (g) Li, L. Q.; Gao, P.; Baumgarten, M.; Müllen, K.; Lu, N.; Fuchs, H.; Chi, L. F. *Adv. Mater.* **2012**, *25*, 3419. (h) Takeda, Y. H.; Andrew, T. L.; Lobez, J. M.; Mork, A. J.; Swager, T. M. *Angew. Chem., Int. Ed.* **2012**, *51*, 9042.

(3) (a) Zhao, Y.; Guo, Y. L.; Liu, Y. Q. *Adv. Mater.* **2013**, *25*, 5372. (b) Li, Y.; Sonar, P.; Murphy, L.; Hong, W. *Energy Environ. Sci.* **2013**, *6*, 1684. (c) Gao, X. K.; Hu, Y. B. *J. Mater. Chem. C* **2014**, DOI: 10.1039/c3tc32046d. (d) Liu, Y.-Y.; Song, C.-L.; Zeng, W.-J.; Zhou, K.-G.; Shi, Z.-F.; Ma, C.-B.; Yang, F.; Zhang, H.-L.; Gong, X. *J. Am. Chem. Soc.* **2010**, *132*, 16349. (e) Lee, T.-H.; Wu, K.-Y.; L, T.-Y.; Wu, J.-S.; Wang, C.-L.; Hsu, C.-S. *Macromolecules* **2013**, *46*, 7687. (d) Yuan, Y. B.; Giri, G.; Ayzner, A. L.; Zoombelt, A. P.; Mannsfeld, S. C. B.; Chen, J. H.; Nordlund, D.; Toney, M. F.; Huang, J. S.; Bao, Z. N. *Nat. Commun.* **2013**, *5*, 3005.

(4) (a) Schwartz, G.; Tee, B. C.-K.; Mei, J. G.; Appleton, A. L.; Kim, D. H.; Wang, H. L.; Bao, Z. N. *Nat. Commun.* **2013**, *4*, 1859. (b) Zhang, L.; Wang, H. L.; Zhao, Y.; Guo, Y. L.; Hu, W. P.; Yu, G.; Liu, Y. Q. *Adv. Mater.* **2013**, *25*, 5455. (c) Chad Webb, R.; Bonifas, A. P.; Behnaz, A.; Zhang, Y. H.; Yu, K. J.; Cheng, H. Y.; Shi, M. X.; Bian, Z. G.; Liu, Z. J.; Kim, Y.-S.; Yeo, W.-H.; Park, J. S.; Song, J. Z.; Li, Y. H.; Huang, Y. G.; Gorbach, A. M.; Rogers, J. A. *Nat. Mater.* **2013**, *12*, 938.

(5) (a) Kang, I.; An, T. K.; Hong, J.-a; Yun, H.-J.; Kim, R.; Chung, D. S.; Park, C. E.; Kim, Y.-H.; Kwon, S.-K. *Adv. Mater.* **2013**, *25*, 524. (b) Kim, R.; Amegadze, P. S. K.; Kang, I.; Yun, H.-J.; Noh, Y.-Y.; Kwon, S.-K.; Kim, Y.-H. *Adv. Funct. Mater.* **2013**, *23*, 5719. (c) Lei, T.; Dou, J.-H.; Cao, X.-Y.; Wang, J.-Y.; Pei, J. *Adv. Mater.* **2013**, *25*, 6589. (d) Fei, Z. P.; Gao, X.; Smith, J.; Pattanasattayavong, P.; Domingo, E. B.; Stingelin, N.; Watkins, S. E.; Anthopoulos, T. D.; Kline, R. J.; Heeney, M. *Chem. Mater.* **2013**, *25*, 59. (e) Qu, S.; Tian, H. *Chem. Commun.* **2012**, *48*, 3039. (f) Li, Y. X.; Zou, J. Y.; Yip, H.-L.; Li, C.-Z.; Zhang, Y.; Cheuh, C.-C.; Inermann, J.; Xu, Y.; Liang, P.-W.; Chen, Y.; Jen, A. K.-Y. *Macromolecules* **2013**, *46*, 5497. (g) Lu, S. F.; Drees, M.; Yao, Y.; Boudinet, D.; Yan, H.; Pan, H. L.; Wang, J.; Li, Y. N.; Usta, H.; Facchetti, A. *Macromolecules* **2013**, *46*, 3895.

(6) (a) Kanimozhi, C.; Yaacobi-Gross, N.; Chou, K. W.; Amassian, A.; Anthopoulos, T.; Patil, S. *J. Am. Chem. Soc.* **2012**, *134*, 16532. (b) Kang, I.; Yun, H.-J.; Chung, D.-S.; Kwon, S. K.; Kim, Y.-H. *J. Am. Chem. Soc.* **2013**, *135*, 14896. (c) Li, J.; Zhao, Y.; Tan, H. S.; Guo, Y. L.; Di, C. A.; Yu, G.; Liu, Y. Q.; Lin, M.; Lim, S. H.; Zhou, Y. H.; Su, H. B.; Ong, B. S. *Sci. Rep.* **2012**, *2*, 1. (d) Lei, T.; Dou, J. H.; Cao, X.; Wang, J.; Pei, J. *Adv. Mater.* **2013**, *25*, 6589. (e) Tseng, H.-R.; Phan, H.; Luo, C.; Wang, M.; Perez, L. A.; Patel, S. N.; Ying, L.; Kramer, E. J.; Nguyen, T.-Q.; Bazan, G. C.; Heeger, A. J. *Adv. Mater.* **2014**, DOI: 10.1002/adma.201305084. (f) Subramaniyan, S.; Kim, F. S.; Ren, G. Q.; Li, H. Y.; Jenekhe, S. A. *Macromolecules* **2012**, *45*, 9029.

(7) (a) Loser, S.; Bruns, C. J.; Miyauchi, H.; Ortiz, R. P.; Facchetti, A.; Stupp, S. I.; Marks, T. J. *J. Am. Chem. Soc.* **2011**, *133*, 8142. (b) Ning, Z. J.; Fu, Y.; Tian, H. *Energy Environ. Sci.* **2010**, *3*, 1170. (c) Lee, O. P.; Yiu, A. T.; Beaujuge, P. M.; Woo, C. H.; Holcombe, T. W.; Millstone, J. E.; Douglas, J. D.; Chen, M. S.; Fréchet, J. M. J. *Adv. Mater.* **2011**, *23*, 5359. (d) Lou, S. L.; Szarko, J. M.; Xu, T.; Yu, L. P.; Marks, T. J.; Chen, L. X. *J. Am. Chem. Soc.* **2011**, *133*, 20661. (e) Henson, Z. B.; Zhang, Y.; Nguyen, T.-Q.; Seo, J. H.; Bazan, G. C. *J. Am. Chem. Soc.* **2013**, *135*, 4163. (f) Jenekhe, S. A.; Lu, L.; Alam, M. M. *Macromolecules* **2001**, *34*, 7315.

(8) Bronstein, H.; Chen, Z. Y.; Ashraf, R. S.; Zhang, W. M.; Du, J. P.; Durrant, J. R.; Tuladhar, P. S.; Song, K.; Watkins, S. E.; Geerts, Y.; Wienk, M. M.; Janssen, R. A. J.; Anthopoulos, T.; Sirringhaus, H.; Heeney, M.; McCulloch, I. *J. Am. Chem. Soc.* **2011**, *133*, 3272.

(9) (a) Tsao, H. N.; Cho, D. M.; Park, I.; Hansen, M. R.; Mavrinskiy, A.; Yoon, D. Y.; Graf, R.; Pisula, W.; Spiess, H. W.; Müllen, K. *J. Am. Chem. Soc.* **2011**, *133*, 2605. (b) Lei, T.; Cao, Y.; Zhou, X.; Peng, Y.; Bian, J.; Pei, J. *Chem. Mater.* **2012**, *24*, 1762. (c) Zhong, H. L.; Li, Z.; Buchaca-Domingo, E.; Rossbauer, S.; Watkins, S. E.; Stingelin, N.; Anthopoulos, T. D.; Heeney, M. *J. Mater. Chem. A* **2013**, *1*, 14973.

(10) Lee, J.; Han, A.-R.; Yu, H.; Shin, T. J.; Yang, C.; Oh, J. H. *J. Am. Chem. Soc.* **2013**, *135*, 9540.

(11) Dutta, G. K.; Han, A.-R.; Lee, J.; Kim, Y.; Oh, J. H.; Yang, C. *Adv. Funct. Mater.* **2013**, *23*, 5317.

(12) (a) Bogert, M.; Ritter, J. *J. Am. Chem. Soc.* **1924**, *46*, 2871. (b) Pechmann, V. H. *Chem. Ber.* **1882**, *15*, 881.

(13) Cai, Z. X.; Guo, Y. L.; Yang, S. F.; Peng, Q.; Luo, H. W.; Liu, Z. T.; Zhang, G. X.; Liu, Y. Q.; Zhang, D. Q. *Chem. Mater.* **2013**, *25*, 471.

(14) Chen, H. J.; Guo, Y. L.; Yu, G.; Zhao, Y.; Zhang, J.; Gao, D.; Liu, H. T.; Liu, Y. Q. *Adv. Mater.* **2012**, *34*, 4618.

(15) (a) Kantchev, E. A. B.; Sullivan, M. B. *Org. Lett.* **2010**, *12*, 4816. (b) Kantchev, E. A. B.; Norsten, T. B.; Tan, M. L. Y.; Ng, J. J. Y.; Sullivan, M. B. *Chem.—Eur. J.* **2012**, *18*, 695.

(16) (a) Carsten, B.; He, F.; Son, H. J.; Xu, T.; Yu, L. P. *Chem. Rev.* **2011**, *111*, 1493. (b) Wang, J. G.; Chen, X.; Cai, Z. X.; Luo, H. W.; Li, Y. H.; Liu, Z. T.; Zhang, G. X.; Zhang, D. Q. *Polym. Chem.* **2013**, *4*, 5283. (c) Li, Y. H.; Zhang, G. X.; Liu, Z. T.; Chen, X.; Wang, J. G.; Di, C. A.; Zhang, D. Q. *Macromolecules* **2013**, *46*, 5504.

(17) The saturation regions of I_{DS} were not obvious for the output curves of OFETs with short channel length (5 μm) and width (1400 μm). But, the saturation regions were detected for these OFETs with long channel length (50 μm) and width (1400 μm) (see Figures S4 and S5). In this case, these OFETs exhibit relatively low hole and electron mobilities. Similar results were reported previously: (a) Reese, C.; Bao, Z. N. *Adv. Funct. Mater.* **2009**, *19*, 763. (b) McCulloch, I.; Heeney, M.; Bailey, C.; Genevicius, K.; Macdonald, I.; Shkunov, M.; Sparrowe, D.; Wanger, R.; Zhang, W. M.; Chabinyc, M. L.; Kline, R. J.; Mcgehee, M. D.; Toney, M. F. *Nat. Mater.* **2006**, *5*, 328.

(18) The performances of **P-BPDTT** were also examined in air, but only *p*-type semiconducting behavior was observed. This may be owing to the fact that LUMO energies of **P-BPDTT** are not low enough and as a result **P-BPDTT** cannot display *n*-type semiconducting behavior in air. In addition, the OFETs with **P-BPDTT** and **P-BPDBT** exhibited good stability in inert atmosphere, and the

carrier mobilities kept almost unchanged by storing the devices in nitrogen for more than 10 days. However, their carrier mobilities dropped quickly after exposure to air.

(19) The hole and electron mobilities were deduced with the following equation: $I_{SD} = \mu C_i(V_G - V_T)^2 W/2L$. They were also deduced with the following equation: $I_{SD} = \mu C_i(V_G - V_T)V_{SD}W/L$ by using the data from the linear region of the output curves. For instance, μ_h and μ_e reached 0.55 $cm^2\ V^{-1}\ s^{-1}$ and 0.23 $cm^2\ V^{-1}\ s^{-1}$, respectively, after annealing at 200 °C for thin film of **P-BPDTT**.

(20) (a) Kim, F. S.; Guo, X. G.; Watson, M. D.; Jenekhe, S. A. *Adv. Mater.* **2010**, *22*, 478. (b) Bijleveld, J. C.; Zoombelt, A. P.; Mathijssen, S. J.; Wienk, M. M.; Turbiez, M.; de Leeuw, D. M.; Janssen, R. A. *J. Am. Chem. Soc.* **2009**, *131*, 16616. (c) Li, H. Y.; Kim, F. S.; Ren, G. Q.; Jenekhe, S. A. *J. Am. Chem. Soc.* **2013**, *135*, 14920.

(21) Guo, X. G.; Kim, F. S.; Seger, M. J.; Jenekhe, S. A.; Watson, M. D. *Chem. Mater.* **2012**, *24*, 1434.

(22) Poelking, C.; Cho, E.; Malafeev, A.; Ivanov, V.; Kremer, K.; Risko, C.; Brédas, J.-L.; Andrienko, D. *J. Phys. Chem. C* **2013**, *117*, 1633.